Cascaded Fractional Control Approach for Frequency Regulation of Multi-Source Power System Integrating Renewable Energy Resources

Shahnawaj
National Institute of Technology, Kurukshetra

Chanana, Saurabh
National Institute of Technology, Kurukshetra

https://doi.org/10.5109/7183377

出版情報：Evergreen. 11 (2), pp.949-963, 2024-06. 九州大学グリーンテクノロジー研究教育センター
バージョン：

Cascaded Fractional Control Approach for Frequency Regulation of Multi-Source Power System Integrating Renewable Energy Resources

Shahnawaj[1,*], Saurabh Chanana[1]
[1]National Institute of Technology, Kurukshetra, Haryana, India

*Author to whom correspondence should be addressed:
E-mail: shahnawaj_6180092@nitkkr.ac.in

(Received December 23, 2023; Revised April 22, 2024; Accepted May 8, 2024).

Abstract: This research article describes the regulation of frequency in an interconnected two-area multi-source power system (MSPS) with the help of fractional order integral (FOI) based controllers. Different configurations of FOI-based controllers were optimized using the recent metaheuristic algorithm wild horse optimization (WHO) and particle swarm optimization (PSO). The model of the problem is defined as having a fitness function based on the integral of time multiplication of absolute error (ITAE) criterion comprising tie-line power and frequency changes. Further, the optimal solution is obtained in terms of the controller gain values. A comparative study in terms of undershoots/overshoots/settling times with several controller configurations has been carried and it was found that the FOI-PIDF controller is superior to other configurations. Additionally, the WHO algorithm has shown better performance as compared to PSO. The simulation results have also been experimentally validated using a real-time simulator based on FPGA. The proposed controller is also compared with other controllers to check its robustness by considering the effect of 2% SLP in both areas and considering the effect of GRC on the system.

Keywords: Wild Horse Optimization (WHO); Load-Frequency-Control (LFC); Field Programmable Gate Arrays (FPGA); Multi-Source Power System (MSPS); Generation Rate Constraint (GRC); Cascaded Controller.

1. Introduction

An interconnected network of various control regions makes up a power system. Power system connectivity is crucial to maintaining the steady flow of power supply and improves system dependability. Load frequency control (LFC) is crucial for the electrical power system to operate stably and dependably. The LFC is in charge of maintaining the system frequency in response to consumers' immediate power needs. At a steady state, the power plant's output ought to be equal to the total load demand less any associated losses. Yet, the nature of the load needs is unpredictable and transient. As a result, generation-demand imbalances suddenly appear. The generator speed varies due to the differential power, which also affects the system frequency. Tie-line power exchange, area frequencies, and area control error (ACE), which is the linear combination of tie-line power and frequency deviations, all depart from the desired values in an interconnected electric power system as load demand fluctuates erratically. To rectify the variations in tie-line power, frequency, ACE, and generation signals under dynamic situations, a suitable, resilient, and intelligent LFC technique is required [1,2].

Fossil fuels are burned in a power system (PS) powered by air or oxygen to create heat and steam, which power turbines to produce electricity. From the dawn of the Industrial Revolution, fossil fuels have been used more and more often. According to recent reports, fossil fuels still provide more than 80% of the world's energy needs, while the world's reserves of the main fossil fuels are running low. On the other side, burning fossil fuels produces poisonous gases as the main byproducts, which are then released into the atmosphere. Such gases are damaging to our planet and act as greenhouse gases, contributing significantly to the global warming that is caused by humans. As a result, several nations have shifted their focus to renewable energy sources (RESs) like solar, geothermal, wind, electrochemical and tidal to mitigate the detrimental consequences of reducing dependence on fossil fuels and rising greenhouse gas concentrations. Following several recent studies in the literature, it has been demonstrated that RESs based on solar thermal generators, aqua-electrolyzer-fuel cells, wind energy systems (WES), dish-Stirling solar thermal systems, solar photovoltaic (PV), and hydro energy

system (HES) significantly improve system performance. The RESs like HESs and WESs units are combined with the PSs that we use in this work, drawing on the potential of the works previously mentioned [3–7].

For the LFC of power systems, several control architectures have been given in the literary text. Initially, due to their simplicity, ordinary integral (I) order controllers have been presented as load frequency controllers, such as proportional integral derivative (PID) and proportional-integral (PI) controllers [8,9]. Soft computing techniques have been used to tune various controllers as a result. Whale optimization algorithm (WOA) [10], PSO [11], bat algorithm [12], marine predator algorithm (MPA) [13], and flower pollination algorithm (FPA) [14] are a few of the optimization approaches that have been used to further study the design of LFC. Multi-area interconnected power networks based on PID controllers have been subject to several LFC proposals. These methods helped the deregulated LFC operation get off the ground. It has been noted that a large number of researchers have concentrated on LFC issues that are specific to the traditional power system. Furthermore, problems such as frequency deviation, voltage instability, reliability issues and poor power quality could result from the large penetration of RES [15–17].

FOI, Fractional order Proportional Integral (FOPI), and Fractional order Proportional Integral Derivative (FOPID) controllers are recommended to ameliorate the performance of traditional I/PI/PID [18–20]. The fractional calculus theory (FCT) is introduced into PID/PI/I controllers in FOPID/FOPI/FOI to improve their results. More tuning parameters on FO controllers provide them more flexibility. In recent years, PS LFC issues have been resolved with FO controllers, which have outperformed conventional controllers in this regard. Some of their implementations are Imperialist Competitive Algorithm (ICA) optimized ITD controller [21], Improved Fitness Dependent Optimizer based FOI-PD [22], Atom Search Optimization optimized FOPID [23] and Big bang big crunch algorithm based FOPID [24].

Currently, in contrast to the single controller structure, the cascaded controller architecture offers greater system performance. As an illustration, cascaded FOPI-FOPD controllers optimized using the dragonfly search algorithm [25], cascaded PI-FOPID controllers based on gorilla troops optimization [26], the cascaded of FOPID-Tilt-integral derivative (TID) controllers optimized using MPA [27], and cascaded fuzzy FOPI-FOPID controllers based on ICA [28] have all been suggested for advanced LFC of PSs to provide better frequency regulation. Parallel to this, WHO, a metaheuristic optimization method based on wild horses' (WHs) social interactions, has recently been investigated [29]. In terms of engineering issue optimization, the WHO algorithm showed good accuracy and efficiency, such as in [30]. Also, by enhancing search capabilities, the WHO algorithm has great potential to produce good results and tolerable performance for several system dimensions. Also, it surpasses other optimization algorithms in all comparable dimensions, whereas the performance of other optimizers noticeably declines as the dimensions rise. The PSO method does have certain drawbacks, though, including the ease with which it can enter a high-dimensional space's local optimum and its slow rate of convergence during repetitive processes [26].

In this paper, a cascaded Fractional Order Integral and Proportional Integral Derivative with Filter (FOI-PIDF) controller is developed for the LFC of interconnected two-area MSPS. Three separate generation sources reheat thermal, hydro, and gas are present in area 1 of the proposed control model, and three generation units reheat thermal, hydro, and wind are present in area 2 as well. Furthermore, a more contemporary meta-heuristic technique called WHO is used to optimize the parameters of the suggested controller. To measure the effectiveness of the suggested controller, a detailed performance comparison is done with the outcomes from PID, PIDF, FOPID, and FOI-PD. gain values optimized using the WHO algorithm and PIDF, FOI-PIDF by PSO algorithm. Further, the system's effectiveness has been examined using ITAE criteria. Finally, it has been proved that the FOI-PIDF controller is more robust by the effect of SLP on both areas and by considering GRC in the thermal and hydro units, and also by RSLP on area1 [22].

This article's remaining sections are ordered as follows. The dynamic system modeling of the proposed interconnected two-area MSPS is presented in Section II. The objective function design and control signal is charted in Section III. The WHO technique for different controller gain values is introduced in Section IV. The simulations of several comparative studies on LFC in MATLAB/SIMULINK and OPAL-RT (OP5700) in the event of load disturbances and discussions on the results obtained are represented in Section V. Finally, the conclusion of the research article is mentioned in Section VI.

2. Dynamic Two-Area Multisource Power System Modeling

In an interconnected two-area MSPS, the load will change very frequently, as a result, a fluctuation in the frequency and deviation in the tie line power is found there. Thus, generators needed to generate less or more electrical energy to cope with the demanded load for the maintenance of scheduled power flow in the tie lines that connect the different areas. When there is less generation as compared to the applied load, then the speed of the generator and thus the frequency will drop, therefore scheduled power levels in the system show changes. The operating limit of the tie-line and the generator is not allowed to exceed and it is ensured by the automatic generation control. Power in the tie-line, speed, and frequency of the generator is used as regulating signals that include the ACE [31].

Figure 1 shows the interconnected two-area MSPS which is considered for the study. The first control area of the rated power is 2000MW and a load of 1500MW comprises of HES, gas energy system (GES) and thermal energy system (TES). However, the second control area with the same rated power and load comprises of HES, WES and TES. The interconnected two-area MSPS is efficiently used in the investigation of the system for the analysis and designing of LFC [32]. The ACE of two-area MSPS is denoted by ACE_{M1} and ACE_{M2}; Frequency bias parameters are represented by B_{M1} and B_{M2}; governor speed regulation parameter is represented by R_i where i can be thermal, gas, hydro or wind; T_{12} shows the tie-line synchronizing coefficient; ΔP_{tie} represents a deviation in tie-line power in pu; ΔF_{M1} and ΔF_{M2} show frequency deviations of the system in pu and ΔP_{L1} and ΔP_{L2} shows the change in load demands. The appendix gives the nominal values of the parameters related to the interconnected two-area MSPS network [33].

The participation factor for each generating unit is provided to evenly distribute the entire load demand amongst all of the generating units. the results unity for any control region that is the total of all participation elements. In actuality, a participation factor of 0.625 is given to the thermal unit, 0.3 to the hydro unit and 0.075 to the gas/wind unit, respectively.

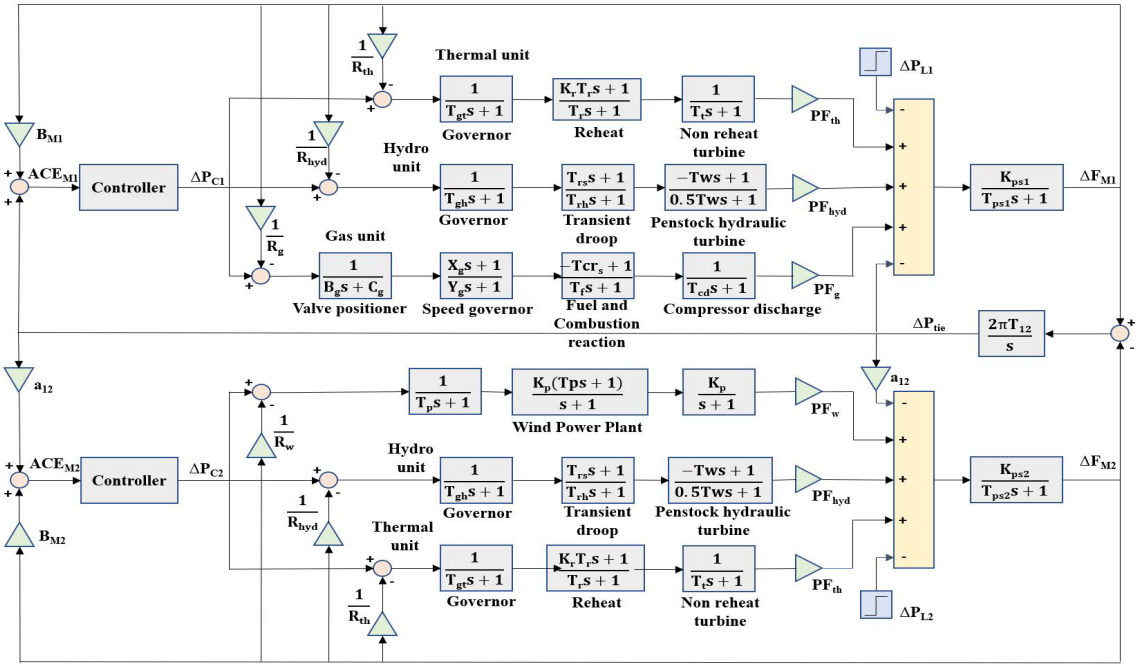

Fig. 1: Interconnected two-area MSPS model.

3. Objective Function Design and Control Signal

In the process industry, the most effective controller for feedback operation is the PID controller. It can give efficient control performance and it is robust despite the continuously varying dynamic behavior of the process plant. For decreasing the peak overshoot values, improving the stability, and ameliorating the transient response of a microgrid system, a derivative controller is used. For decreasing the rise time, a proportional controller is used but it never decreases the steady-state error. The steady-state error is decreased with the help of an integral controller but it may degrade the transient response. PID controllers are the best alternative when fast response and stability are needed. Unlike other controllers, the advantage of the PID controller is that it can help in improving system stability and also for achieving better settling time [34]. In the last few decades, fractional-order controllers attained considerable attention due to a higher disturbance rejection ratio, a lower noise effect, and a shorter calculation time than typical controllers. Nowadays cascaded PID controllers are used which further ameliorate the dynamic performance of the system. Performance analysis of interconnected two-area MSPS is carried out by optimizing the gain values of the FOI-PIDF controller. Controllers such as PID, PIDF, FOPID and FOI-PD represented in Fig. 2 to Fig.5 respectively, were used in the comparison of results to the FOI-PIDF controller which is represented in Fig. 6. The Eq. 1 to Eq. 5, given below represents the PID, PIDF, FOPID, PD and FOI controller's transfer function [35].

$$TF_{PID} = K_p + \frac{K_I}{s} + K_D s \quad (1)$$

$$TF_{PIDF} = K_p + \frac{K_I}{s} + \frac{K_D s N}{s+N} \quad (2)$$

$$TF_{FOPID} = K_p + \frac{K_I}{s^{\lambda}} + K_D s^{\mu} \quad (3)$$

$$TF_{PD} = K_p + K_D s \quad (4)$$

$$TF_{FOI} = \frac{1}{s^{\lambda}} \quad (5)$$

Area-control errors (ACE) are respectively represented by Eq. 6 and Eq. 7, and these are fed to the respective controllers as input.

$$ACE_{M1} = B_{M1}\Delta F_{M1} + \Delta P_{tie} \quad (6)$$
$$ACE_{M2} = B_{M2}\Delta F_{M2} + a_{12}\Delta P_{tie} \quad (7)$$

The respective outputs of the controller are ΔP_{C1} and ΔP_{C2} and these are used as the regulating inputs of the two interconnected MSPS areas respectively. To begin with, a controller is designed based on a recent metaheuristic optimization technique according to the desired constraints and specifications, and this controller is used to calculate the objective function. ITAE, Integral of absolute error (IAE), Integral of time multiplication of squared error (ITSE) and Integral of squared error (ISE) are generally used in the control design for performance criteria. ISE, as well as IAE-based tuning, cannot be used for decreasing settling time therefore, the ITAE criterion is used to reduce it. Peak overshoot is also reduced due to the ITAE criterion. It was proved already that ITAE is a preferable fitness function in the case of LFC studies [36,37]. Thus, an objective function based on the ITAE criterion is used for the optimizing gain values of other controllers in this investigation and the proposed controller. The expression for IAE, ISE, ITSE and ITAE criteria-based fitness function for the proposed system is given below in Eq. 8 to Eq. 11, respectively [38].

$$IAE = \int_0^{t_{sim}} (|\Delta F_{M1}| + |\Delta F_{M2}| + |\Delta P_{Tie}|).dt \quad (8)$$
$$ISE = \int_0^{t_{sim}} ((\Delta F_{M1})^2 + (\Delta F_{M2})^2 + (\Delta P_{Tie})^2).dt \quad (9)$$
$$ITSE = \int_0^{t_{sim}} ((\Delta F_{M1})^2 + (\Delta F_{M2})^2 + (\Delta P_{Tie})^2).t_{sim}.dt \quad (10)$$
$$Y = ITAE = \int_0^{t_{sim}} (|\Delta F_{M1}| + |\Delta F_{M2}| + |\Delta P_{Tie}|).t_{sim}.dt \quad (11)$$

In the above equation, the simulation time range is represented by tsim. The problem constraints of the above equation are gain values of parameter bounds of the controllers. Subsequently, the design problem formulation is represented by the following optimization problem (OP). Minimizes Y (ITAE), subjected to

In Eq. 12, max and min are the maximum and minimum values of respective K_P, K_I, K_D, I, λ, μ and N parameters of controllers used in this study. The constraint set for K_P, K_I, K_D and I is [-5,5]; λ and μ is [0,1] and for N is [100,500] which is chosen after a comprehensive trial and error method.

$$\left.\begin{array}{l} K_P^{min} \le K_P \le K_P^{max} \\ K_I^{min} \le K_I \le K_I^{max} \\ K_D^{min} \le K_D \le K_D^{max} \\ I^{min} \le I \le I^{max} \\ \lambda^{min} \le \lambda \le \lambda^{max} \\ \mu^{min} \le \mu \le \mu^{max} \\ N^{min} \le N \le N^{max} \end{array}\right\} \quad (12)$$

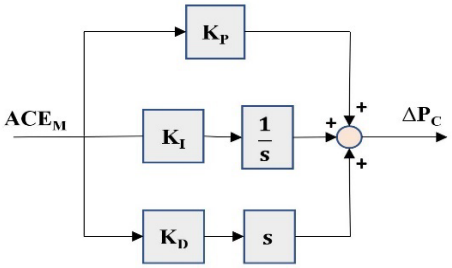

Fig. 2: PID controller

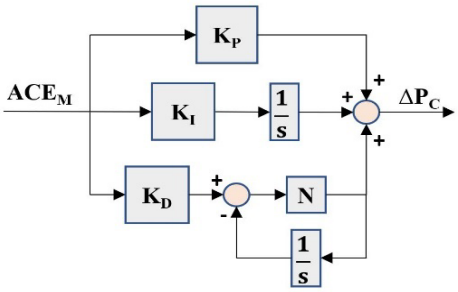

Fig. 3: PIDF controller

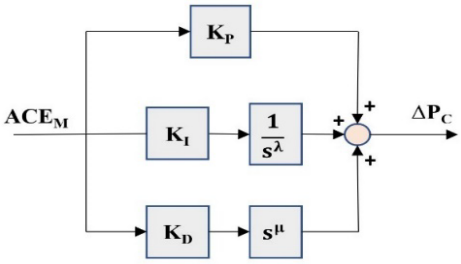

Fig. 4: FOPID controller

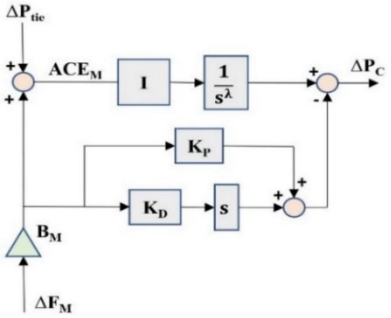

Fig. 5: FOI-PD controller

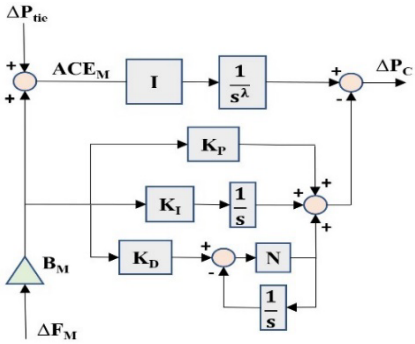

Fig. 6: FOI-PIDF controller

4. Optimization Algorithm

4.1 Wild Horse Optimization Method

WHO is a newly generated metaheuristic algorithm that is based on how WHs interact with one another [29]. WHs are employed in this approach to represent diverse behaviors like mating, grazing, hunting, chasing and leading. Although communities within WHs are either territorial or non-territorial, the WHO technique is based on the non-territorial groups, which are composed of the group's stallion, leader mare or leaders, and their progeny. The stallion's responsibility is to lead the herd and communicate with the mares because the foals begin their lives grazing. Foals also leave their families and join others when they reach adulthood. The WHO procedure can be summed up using the stages stated below:

4.2 Mathematical Model

The various steps used by the WHs are replicated and simulated by the WHO's mathematical model. It consists of the following five main steps:

- First step: population initialization
- Second step: grazing behavior
- Third step: WH mating behavior
- Fourth step: group leadership
- Fifth step: leaders exchange and selection

The WHO's theory is thoroughly explained in [39], and the ensuing Eq. 13 to Eq. 18, are used to represent the WHs' behavior. The flow chart of the WHO algorithm is represented in Fig. 7.

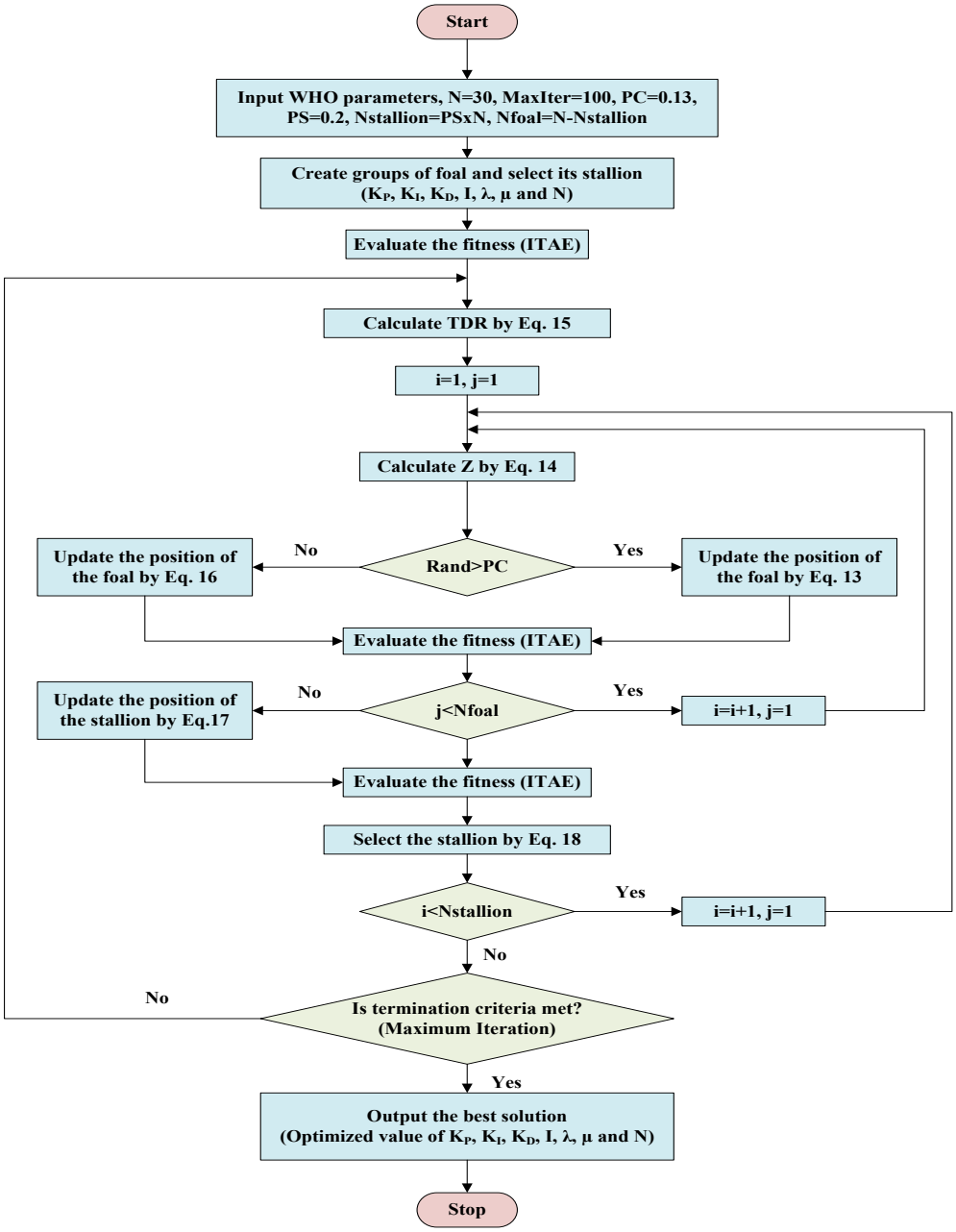

Fig. 7: Flowchart of WHO algorithm.

$$\bar{X}_{i,G}^{j} = 2Z\cos(2\pi RZ)\left(Stallion^{j} - X_{i,G}^{j}\right) + Stallion^{j} \quad (13)$$

$$P = \overrightarrow{R_1} < TDR;\ IDX = (P == 0);$$
$$Z = R_2 \Theta IDX + \overrightarrow{R_3}\Theta(\sim IDX) \quad (14)$$

$$TDR = 1 - iter\left(\frac{1}{iter_{max}}\right) \quad (15)$$

$$X_{K,G}^{p} = Crossover\left(X_{G,i}^{q}, X_{G,j}^{z}\right), i \neq j \neq k, p = q = end,$$
$$Crossover = mean \quad (16)$$

$$\overline{Stallion_{G_i}} = \begin{Bmatrix} 2Z\cos(2\pi RZ)\left(WH - Stallion_{G_i}\right) + WH & if\ R_3 > 0.5 \\ 2Z\cos(2\pi RZ)\left(WH - Stallion_{G_i}\right) - WH & if\ R_3 \leq 0.5 \end{Bmatrix} \quad (17)$$

$$Stallion_{G_i} = \begin{Bmatrix} X_{G,i}\ if\ \cos\left(X_{G,i}\right) < \cos t(Stallion_{G_i}) \\ Stallion_{G_i}\ if\ \cos\left(X_{G,i}\right) > \cos t(Stallion_{G_i}) \end{Bmatrix} \quad (18)$$

Where the symbols *i*, *j*, *Stallion* $_j$, and *WH*, are the group member number, total stallion number, spot of stallion, and waterhole location, respectively. The $X_{K,G}^{p}$, $X_{G,i}^{q}$ and $X_{G,j}^{z}$ are the *WH p* position of the *k* group, *i* group's foal *q*, and *j* group's foal *z*, respectively. All of ($Stallion_{G_i}$, $\overline{Stallion_{G_i}}$), and ($X_{i,G}^{j}$, $\bar{X}_{i,G}^{j}$) represents the current and next iteration place of the leader of the group *i*, and group member, respectively. A randomly chosen adaptive mechanism is represented by *Z*. *R* is the arbitrary number in the range of [−2, 2]. *P* is a vector comprised of 0 and 1 equivalent to problem dimensions. $\overrightarrow{R_1}$, and $\overrightarrow{R_3}$ are in the range of [0,1] represents random uniform distribution vectors, R_2 is also having same range represents random uniform distribution number. *IDX* is the index of $\overrightarrow{R_1}$. *TDR* starts with 1 and lessens the process [40].

5. Simulation Results and Analysis

This section discusses the two-area hybrid system's performance under various uncertainties, including SLP (step load perturbation) in area 1, SLP in both areas, random load variation, and GRC (generation rate constraints). For each scenario, the cascaded FOI-PIDF controller is compared with the other controllers utilizing the PSO and WHO algorithms. The resulting values of the ITAE objective function, the time response, and the dynamic specifications of the tie-line power and frequency variations are all included in this comparison. For the dynamic response characteristics (DRC) of the interconnected two-area MSPS, the regulating parameters of the WHO algorithm can be taken as total population (N) = 30, stallion percentage (PS) = 0.2, crossover percentage (PC) = 0.13, maximum-iteration = 100 for each case. The appendix gives the nominal values of the parameters related to the interconnected two-area MSPS network [32].

5.1 Effect of Step Load Perturbation in Area 1

The interconnected two-area MSPS is contemplated with different controllers. The model of this system is generated in MATLAB/SIMULINK. The program of OP using WHO and PSO is written in a .m file. In this aforementioned study, the gain values of different controllers are taken as the constraint of the OP denoted by Eq. 12. The objective function of OP is based on the ITAE criterion which is denoted by Eq. (11) and an increase in step load by 2% in area 1 is applied to the model. Table 1 shows the optimized gain values of FOI-PIDF, FOI-PD, FOPID, PIDF and PID controller using the WHO algorithm and FOI-PIDF and PIDF controller using the PSO algorithm, which we have evaluated after running the respective programs. Initially, the different controller's gain values obtained by the PSO and WHO algorithms are simulated for the FOI-PIDF and PIDF controllers. DRC of the respective system are represented by Figs. 8(a)-8(c). Table 2 shows the corresponding performance indicators concerning peak undershoot, peak overshoot and settling time calculated for the deviation of power in the tie line and frequency deviation of area 1 and area 2 of the system. ITAE values of the controllers optimized using WHO and PSO discussed above are also represented in Table 2. The gain values of the WHO-optimized cascaded FOI-PIDF controller produce better results for the ITAE criterion. This shows the superiority of WHO in calculating controller gain values over PSO.

In the next analysis, the FOI-PIDF, FOI-PD, FOPID and PID controller gain values optimized using WHO are compared. DRC of the respective system are represented by Figs. 9(a)-9(c). Table 3 shows the corresponding performance indicators concerning peak undershoot, peak overshoot and settling time calculated for the deviation of power in the tie line and frequency deviation of area 1 and area 2 of the system. ITAE values of all the controllers optimized using WHO discussed above are also represented in Table 3. Outcomes of the results suggest that the FOI-PIDF controller gain values optimized using WHO offer better dynamic characteristics for the ITAE criterion. The estimated index demonstrates that the cascaded FOI-PIDF controller is superior to the others.

On an FPGA-based OPAL-RT (OP-5700) as shown in Fig.10, real-time simulation is conducted with hardware in loop (HIL). In HIL simulation, a computer model that is identical to the physical plant that interfaces with other equipment and control systems replaces the physical plant. The simulation time in real-time simulation is independent of the host PC's timer. Its timer is in sync with an actual clock. A fixed-time step is used in real-time simulation. At least two subsystems are required for any model that runs in OPAL-RT. The console connects to the PC in real-time, while the master is synced in real-time. The interaction between the user and the model parameters in real-time is created with the help of the console subsystem while viewing the output signals through DSO [41]. The same controllers and gain values

which are given in Table 1 are also taken in the case of real-time simulation. The FOI-PIDF and PIDF controller gain values optimized using WHO and PSO, and the DRC of the respective system are represented by Figs. 11(a)-11(c). Table 4 shows the real-time performance of the optimized system showing peak undershoot and peak overshoot calculated for the deviation of power in the tie line and fluctuation in the frequency of area 1 and area 2 of the system. The FOI-PIDF, FOI-PD, FOPID and PID controller gain values optimized using WHO and the DRC of the respective system are represented by Figs. 12(a)-12(c). Table 5 shows the real-time performance of the optimized system showing peak undershoot and peak overshoot calculated for the deviation of power in the tie line and fluctuation in the frequency of area 1 and area 2 of the system. Outcomes of the real-time simulation suggest that the FOI-PIDF controller gain values optimized using WHO offer a better response.

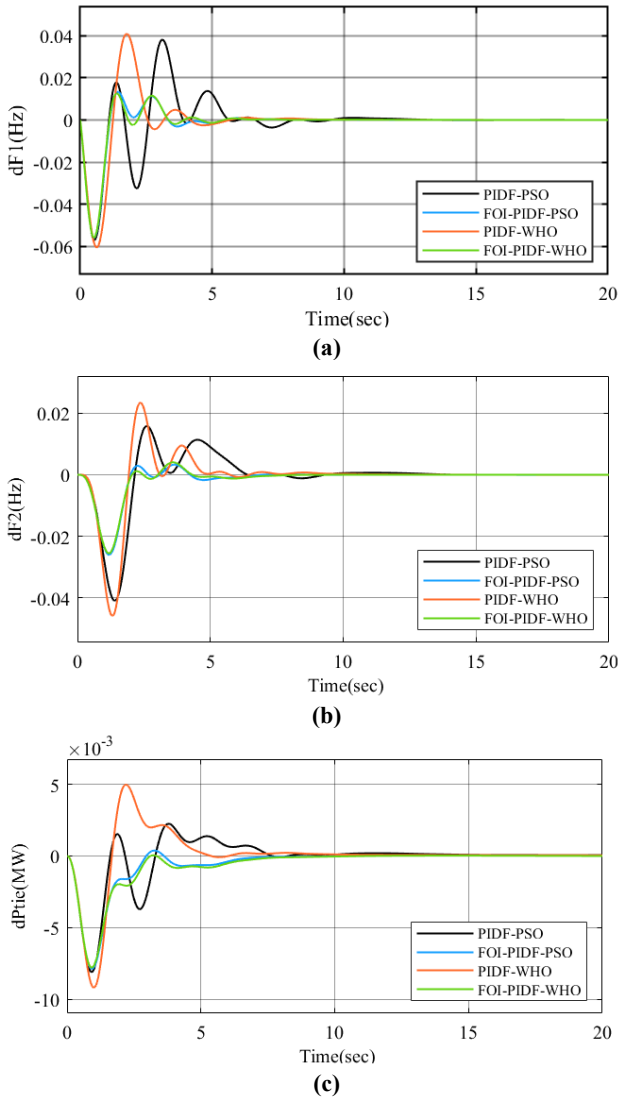

Fig. 8: Comparative performance of PSO and WHO for PIDF and FOI-PIDF controller for 2% SLP in area1, fluctuation in (a) Frequency in area1 (b) Frequency in area2 (c) Tie line power.

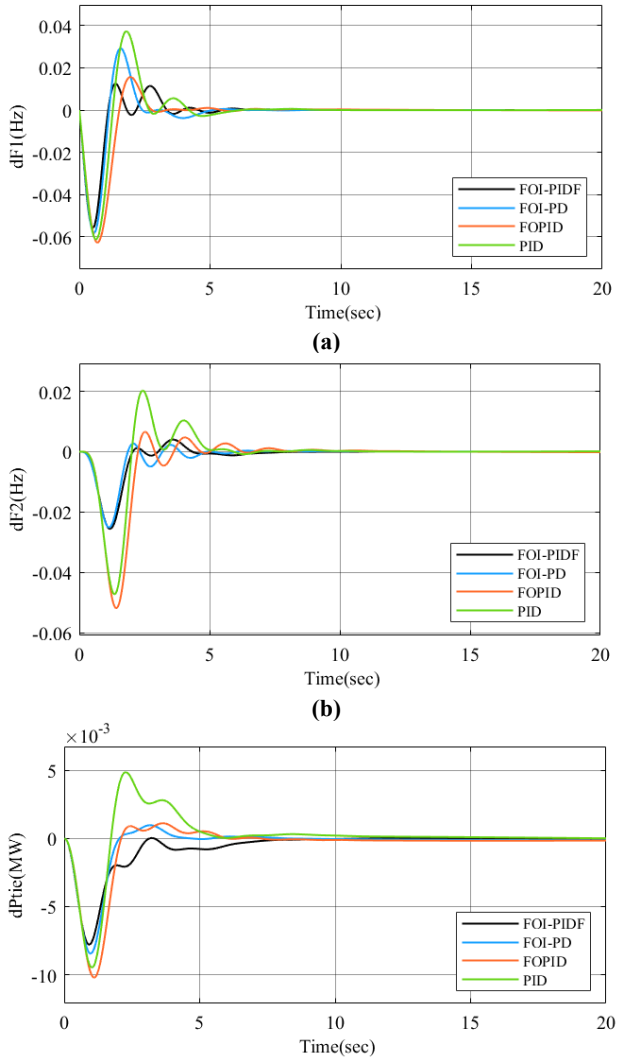

Fig. 9: Comparative performance of WHO for different controllers for 2% SLP in area1, fluctuation in (a) Frequency in area1 (b) Frequency in area2 (c) Tie line power.

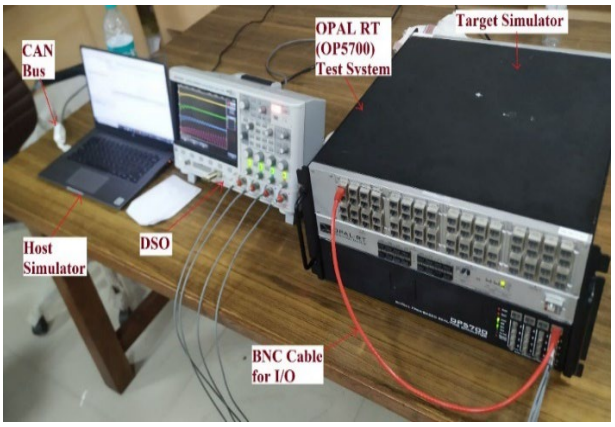

Fig. 10: OPAL-RT (OP5700) Laboratory setup.

Table 1. Optimal gain values of different controllers by WHO and PSO techniques for 2% SLP in area1.

Controller/ Parameters	PIDF-PSO	FOI-PIDF-PSO	PID-WHO	PIDF-WHO	FOPID-WHO	FOI-PD-WHO	FOI-PIDF-WHO
K_{P1}	-1.51	0.54	-1.53	-1.76	-0.01	1.75	0.76
K_{I1}	-2.69	1.48	-3.64	-3.99	-2.65	-	1.5
K_{D1}	-2.55	2.85	-1.63	-1.71	-1.52	2.44	2.89
N1	403	374	-	232	-	-	500
I1	-	-3.41	-	-	-	-4.24	-3.14
λ1	-	0.43	-	-	0.65	0.66	0.43
μ1	-	-	-	-	0.93	-	-
K_{P2}	-1.46	0.67	1.53	1.29	0.42	0.34	0.76
K_{I2}	0.12	-0.01	-0.03	-0.01	0.13	-	0.07
K_{D2}	-0.96	2.38	-2.8	-2.93	-2.72	2.9	2.29
N2	273	360	-	497	-	-	446
I2	-	-2.16	-	-	-	0.97	-1.63
λ2	-	0.45	-	-	0.29	0.19	0.65
μ2	-	-	-	-	1	-	-

Table 2. Transient performance of optimized PIDF and FOI-PIDF controllers using PSO and WHO algorithms for 2% SLP in area1.

Controller/ Parameters	Peak undershoot x 10^{-2}			Peak overshoot x 10^{-2}			Settling time(sec)			ITAE
	ΔF_{M1} (pu)	ΔF_{M2} (pu)	ΔP_{Tie} (pu)	ΔF_{M1} (pu)	ΔF_{M2} (pu)	ΔP_{Tie} (pu)	ΔF_{M1}	ΔF_{M2}	ΔP_{Tie}	
PIDF-PSO	-5.70	-4.10	-0.81	3.80	1.59	0.225	7.82	8.80	7.38	0.534
FOI-PIDF-PSO	-5.60	-2.61	-0.79	1.33	0.33	0.038	5.21	6.34	6.74	0.162
PIDF-WHO	-6.06	-4.59	-0.92	4.08	2.35	0.498	5.28	6.98	5.00	0.326
FOI-PIDF-WHO	-5.58	-2.56	-0.78	1.25	0.41	0.005	5.13	6.76	7.40	**0.154**

Table 3. Transient performance of different controllers optimized using WHO algorithm for 2% SLP in area1.

Controller/ Parameters	Peak undershoot x 10^{-2}			Peak overshoot x 10^{-2}			Settling time(sec)			ITAE
	ΔF_{M1} (pu)	ΔF_{M2} (pu)	ΔP_{Tie} (pu)	ΔF_{M1} (pu)	ΔF_{M2} (pu)	ΔP_{Tie} (pu)	ΔF_{M1}	ΔF_{M2}	ΔP_{Tie}	
PID	-6.13	-4.72	-0.95	3.73	2.02	0.487	5.51	6.37	10.20	0.334
FOPID	-6.28	-5.19	-1.02	1.57	0.66	0.112	2.69	7.55	7.05	0.288
FOI-PD	-5.82	-2.51	-0.84	2.93	0.27	0.097	4.72	5.77	7.85	0.166
FOI-PIDF	-5.58	-2.56	-0.78	1.25	0.41	0.005	5.13	6.76	7.40	**0.154**

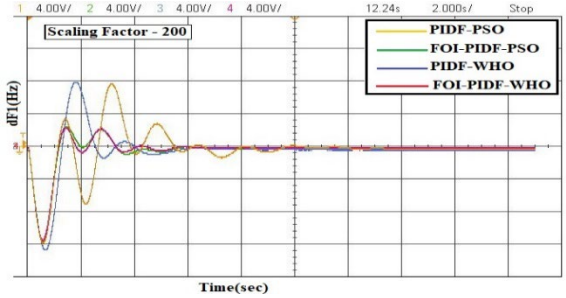

(a)

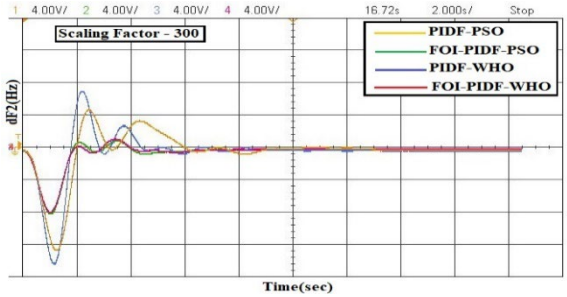

(b)

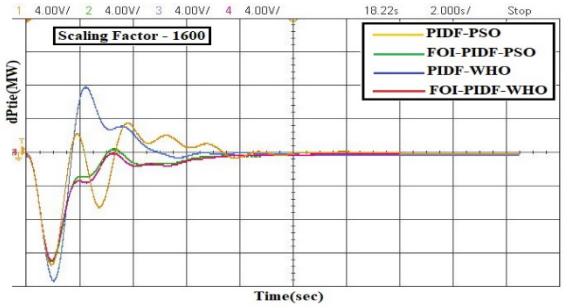

(c)

Fig. 11: Comparative performance of PSO and WHO for PIDF and FOI-PIDF controller in real-time for 2% SLP in area1, fluctuation in (a) Frequency in area1 (b) Frequency in area2 (c) Tie line power.

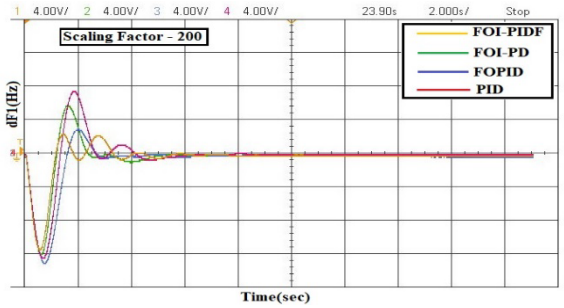

(a)

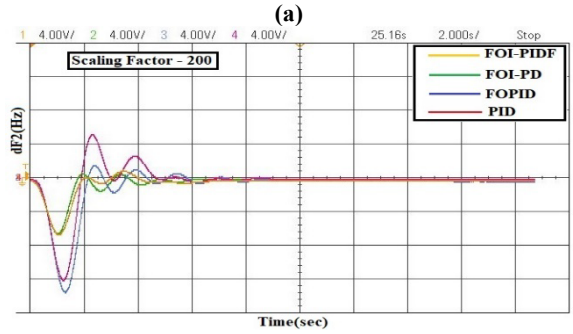

(b)

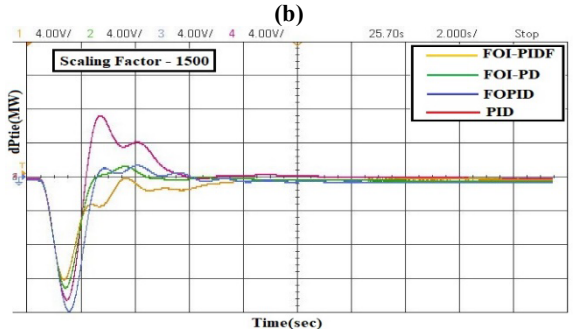

(c)

Fig. 12: Comparative performance of WHO for different controllers in real-time for 2% SLP in area1, fluctuation in (a) Frequency in area1 (b) Frequency in area2 (c) Tie line power.

5.2 Effect of Step Load Perturbation in Both Areas

The interconnected two-area MSPS contemplated in section 5.1 is again analyzed in this section, however, an SLP of 2% is applied in both areas to further compare the robustness of proposed controllers and algorithms. Table 6 shows the optimized gain values of FOI-PIDF, FOI-PD and FOPID controller using the PSO algorithm and FOI-PIDF controller using the WHO algorithm which we have evaluated after running the respective program. The objective function of the OP is based on the ITAE criterion as given by Eq. 11 and an increase in step load by 2% in both areas is applied to the system and the different controller's gain values by the respective methods are calculated for the model by running simulation. DRC of the respective system are represented by Figs. 13(a)-13(c).

Table 4. Transient performance of optimized PIDF and FOI-PIDF controllers using PSO and WHO algorithms in real-time.

Controller/ Parameters	Peak undershoot x 10^{-2}			Peak overshoot x 10^{-2}		
	ΔF_{M1} (pu)	ΔF_{M2} (pu)	ΔP_{Tie} (pu)	ΔF_{M1} (pu)	ΔF_{M2} (pu)	ΔP_{Tie} (pu)
PIDF-PSO	-5.72	-4.15	-0.82	3.95	1.63	0.240
FOI-PIDF-PSO	-5.63	-2.62	-0.79	1.36	0.37	0.042
PIDF-WHO	-6.16	-4.66	-0.93	4.12	2.43	0.516
FOI-PIDF-WHO	-5.62	-2.57	-0.79	1.21	0.43	0.009

Table 5. Transient performance of different controllers optimized using WHO algorithm in real-time.

Controller/ Parameters	Peak undershoot x 10^{-2}			Peak overshoot x 10^{-2}		
	ΔF_{M1} (pu)	ΔF_{M2} (pu)	ΔP_{Tie} (pu)	ΔF_{M1} (pu)	ΔF_{M2} (pu)	ΔP_{Tie} (pu)
PID	-6.19	-4.78	-0.95	3.80	2.12	0.497
FOPID	-6.39	-5.26	-1.03	1.58	0.71	0.116
FOI-PD	-5.89	-2.54	-0.85	2.96	0.28	0.099
FOI-PIDF	-5.62	-2.57	-0.79	1.21	0.43	0.009

Table 6. Optimal gain values of FOI-PIDF, FOI-PD and FOPID controller using PSO and FOI-PIDF using WHO for 2% SLP in both the areas.

Controller/ Parameters	FOPID-PSO	*FOI-PD-PSO*	FOI-PIDF-PSO	*FOI-PIDF-WHO*
K_{P1}	-0.31	2.73	2.74	2.70
K_{I1}	-3.44	-	-1.29	-2.12
K_{D1}	-1.43	2.72	2.74	2.51
N1	-	-	302	263
I1	-	-3.28	-4.58	-4.90
λ1	0.65	0.77	0.85	0.89
μ1	0.97	-	-	-
K_{P2}	0.25	0.80	0.66	-0.80
K_{I2}	-1.82	-	0.78	-0.90
K_{D2}	-2.76	3.18	2.96	2.96
N2	-	-	293	496
I2	-	-5	-2.66	-4.32
λ2	0.64	0.62	0.42	0.26
μ2	1	-	-	-

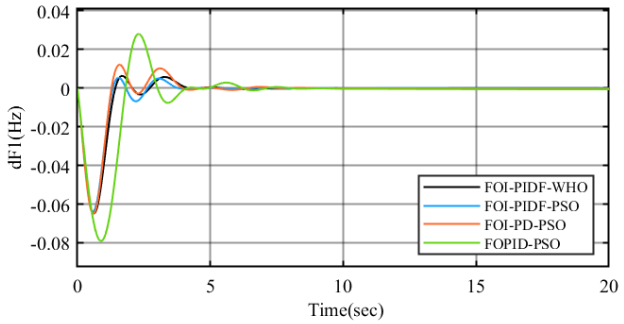

(a)

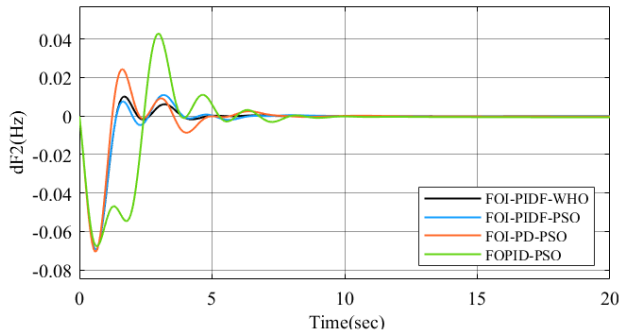

(b)

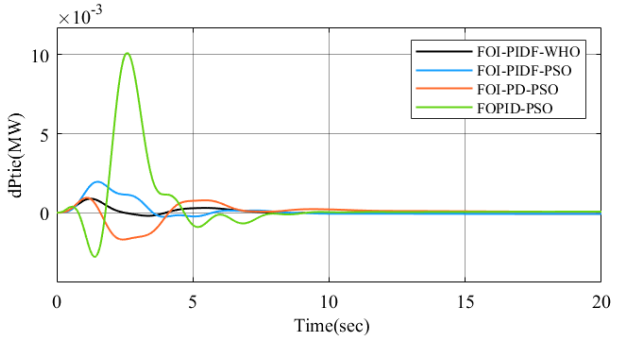

(c)

Fig. 13: Comparative performance of PSO and WHO for different controllers for 2% SLP in both the areas, fluctuation in (a) Frequency in area1 (b) Frequency in area2 (c) Tie line power.

Outcomes of the simulation suggest that the FOI-PIDF controller gain values optimized using WHO offer better dynamic characteristics. Table 7 shows the corresponding performance indicators concerning peak undershoot, peak overshoot and settling time calculated for the deviation of power in the tie line and frequency deviation of area 1 and area 2 of the system. ITAE values of the controllers optimized using WHO and PSO discussed above are also represented in Table 7. The gain values of the WHO-optimized cascaded FOI-PIDF controller produce better results as compared to other configurations. The performance index also demonstrates that the cascaded FOI-PIDF controller is superior to the others.

5.3 Effect of Generation Rate Constraint

For the realization of non-linearity, the hydro system and the thermal system in each area are restricted with GRC. The thermal system's GRC of 3% per minute is chosen for this analysis for both increasing and decreasing generation. For an increasing generation in the hydro system, a GRC of 270% per minute is chosen, while for a decreasing generation, a GRC of 360% per minute is used [42]. The interconnected two-area MSPS is studied and discussed in previous sections 5.1 and 5.2. Table 8 shows the optimized gain values of FOI-PIDF, FOI-PD and FOPID controller using the PSO algorithm and FOI-PIDF controller using the WHO algorithm which we have evaluated after running the respective program. The gain values of different controllers are taken as the constraint of the OP denoted by Eq. 12. The objective function is based on the ITAE criterion as given by Eq. 11 and an increase in step load by 2% in area 1 is applied to the system and the different controller's gain values by the respective method are calculated for the developed model by running simulation. DRC of the respective system are represented by Figs. 14(a)-14(c).

Table 7. Transient performance of different controllers optimized using PSO and WHO algorithm for 2% SLP in both areas.

Controller/ Parameters	Peak undershoot x 10^{-2}			Peak overshoot x 10^{-2}			Settling time(sec)			ITAE
	ΔF_{M1} (pu)	ΔF_{M2} (pu)	ΔP_{Tie} (pu)	ΔF_{M1} (pu)	ΔF_{M2} (pu)	ΔP_{Tie} (pu)	ΔF_{M1}	ΔF_{M2}	ΔP_{Tie}	
FOI-PIDF-WHO	-6.51	-6.93	-0.020	0.63	1.02	0.088	3.92	4.43	12.45	**0.155**
FOI-PIDF-PSO	-6.40	-6.94	-0.026	0.55	1.10	0.196	3.59	5.91	9.13	0.179
FOI-PD-PSO	-6.53	-7.06	-0.170	1.22	2.44	0.095	3.84	6.98	14.79	0.294
FOPID-PSO	-7.91	-6.77	-0.280	2.80	4.29	1.102	6.06	7.58	7.65	0.693

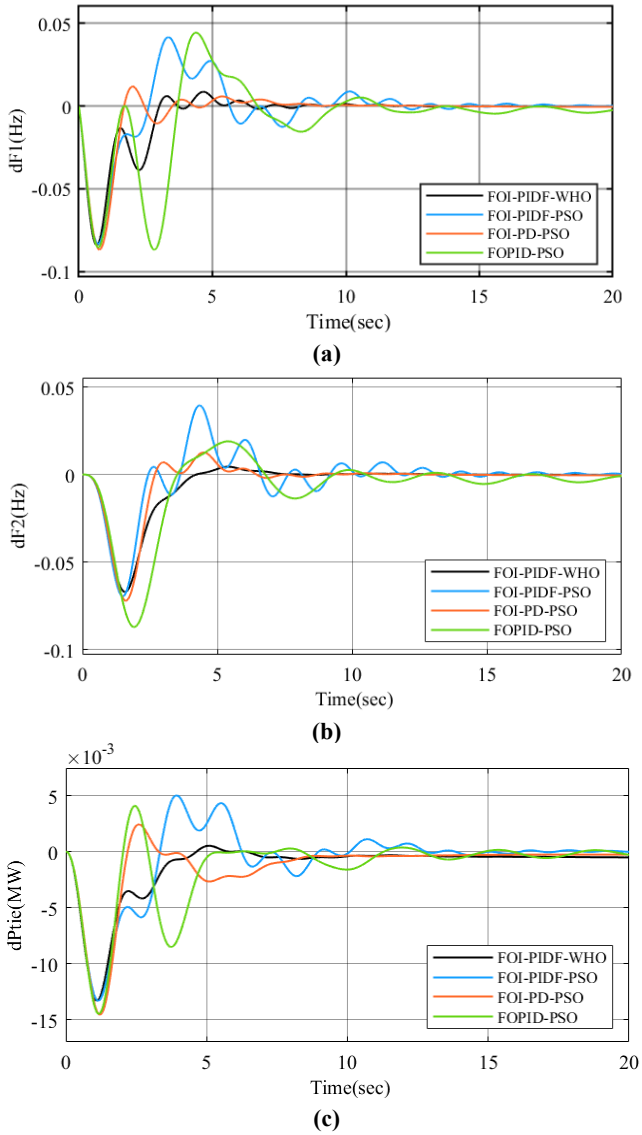

Fig. 14: Comparative performance of PSO and WHO for different controllers for 2% SLP in area1 when GRC is considered, fluctuation in (a) Frequency in area1 (b) Frequency in area2 (c) Tie line power.

In this case, too, simulation suggests that the FOI-PIDF controller gain values optimized using WHO deliver better dynamic characteristics. Table 9 shows the ITAE values of all the controllers and corresponding performance indicators concerning peak undershoot, peak overshoot and settling time calculated for the deviation of power in the tie line and frequency deviation of area 1 and area 2 of the simulated system. The results obtained after dynamic performance analysis clearly suggest that the WHO-optimized FOI-PIDF controller shows better results in case the system has GRC.

5.4 Effect of Random Step Load Pattern in Area 1

In LFC of MSPS, SLP represents typical operational conditions, which can vary due to factors like load characteristics, generation profiles, and other system parameters. These variations directly affect system frequency and stability, impacting simulation parameters such as load demand, frequency fluctuations, and control response. Robustness is key for controllers to maintain stability amid these changes. A robust controller must adapt to different SLPs without losing effectiveness. Optimization algorithms that fine-tune these controllers must also account for SLP variations to ensure consistent performance. The impact of SLP variations can be significant: they might lead to reduced stability margins, longer settling times, greater overshoot, or even system instability. To ensure robustness in LFC, controllers should be designed with adaptability, comprehensive testing should be conducted across varied SLP scenarios, and optimization algorithms must ensure resilience against SLP variations.

To perform additional analysis, the effect of random load variation from 0 to 5% in area1 is analysed on change in frequency of both areas and tie line power. The FOI-PIDF controller gain value optimized using WHO of the interconnected two-area MSPS given in Table 1 and the DRC of the controller are obtained in MATLAB/SIMULINK are given in Fig. 15. FOI-PIDF controller gain values optimized with the help of WHO technique value provide enhanced system stability. Also, the figures demonstrate the beneficial effect in terms of reduced frequency peak and variations and deviations of power in the tie line. The results obtained after dynamic performance analysis confirmed the robustness of the proposed controller and algorithm under different conditions, and this time, considering RSLP. Consequently, it can be concluded that the controller is robust and effective.

Table 8. Optimal gain values of FOI-PIDF, FOI-PD and FOPID controller using PSO and FOI-PIDF using WHO for 2% SLP in area1 when GRC is considered.

Controller/ Parameters	**FOPID -PSO**	***FOI-PD-PSO***	**FOI-PIDF-PSO**	***FOI-PIDF-WHO***
K_{P1}	2.48	1.97	3.26	1.38
K_{I1}	-4.91	-	5.00	-1.37
K_{D1}	-3.62	2.63	2.91	3.46
N1	-	-	360	216
I1	-	-3.80	1.45	-4.03
λ1	0.47	0.64	0.05	0.76
μ1	0.90	-	-	-
K_{P2}	-0.28	-1.14	1.66	1.27
K_{I2}	-0.94	-	-0.20	0.13
K_{D2}	0.12	3.08	3.18	1.89
N2	-	-	215	205
I2	-	-2.34	-0.34	0.68
λ2	0	0.28	0.37	0.01
μ2	0.96	-	-	-

Table 9. Transient performance of different controllers optimized using PSO and WHO algorithm when GRC is considered.

Controller/ Parameters	Peak undershoot x 10^{-2}			Peak overshoot x 10^{-2}			Settling time(sec)			ITAE
	ΔF_{M1} (pu)	ΔF_{M2} (pu)	ΔP_{Tie} (pu)	ΔF_{M1} (pu)	ΔF_{M2} (pu)	ΔP_{Tie} (pu)	ΔF_{M1}	ΔF_{M2}	ΔP_{Tie}	
FOI-PIDF-WHO	-8.40	-6.71	-1.33	0.87	0.44	0.052	6.28	6.98	6.72	**0.618**
FOI-PIDF-PSO	-8.33	-6.96	-1.33	4.17	3.95	0.501	14.00	14.86	14.51	1.550
FOI-PD-PSO	-8.69	-7.21	-1.46	1.18	1.26	0.243	8.44	6.90	8.37	0.634
FOPID-PSO	-8.69	-8.72	-1.45	4.44	1.90	0.409	17.69	19.27	19.38	2.425

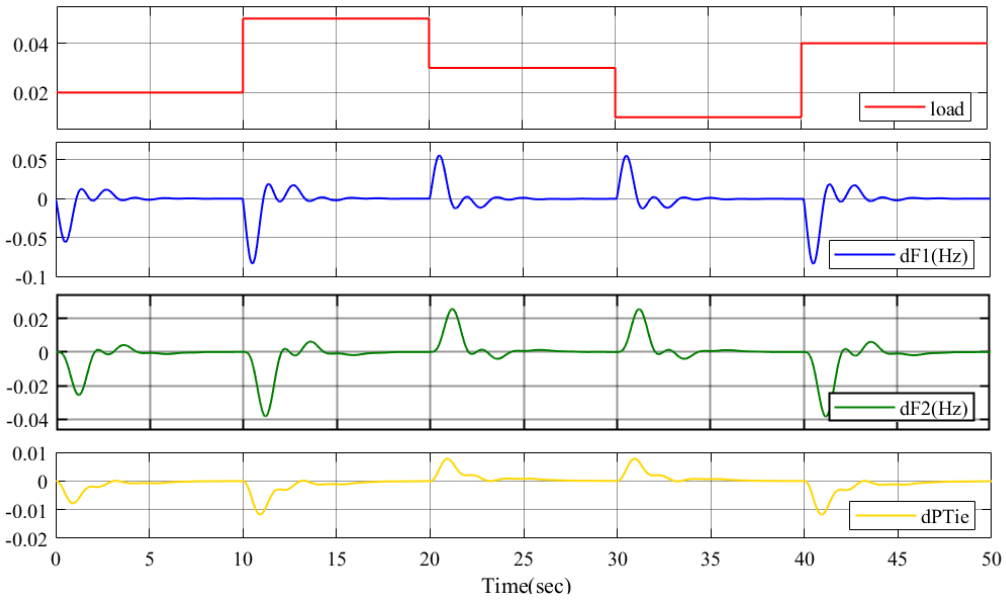

Fig .15: Dynamic responses under RSLP in area1, dF1, dF2 and dPtie.

6. Conclusion

The article delves into a study on LFC of interconnected two-area MSPS under varying conditions. It utilizes a specialized software environment to implement a cascaded FOI-PIDF controller, showcasing its ability to notably enhance system performance amidst uncertainties. A newly developed optimization algorithm, the WHO, is employed to achieve optimal gains for the controller. The study evaluates the system's dynamic responses by comparing it with various controllers and optimization algorithms using simulations conducted in MATLAB/Simulink and HIL on an FPGA-based real-time simulator (OP5700). Results demonstrate significant improvements in dynamic characteristics, with parameters like settling time, peak undershoot, peak overshoot, and ITAE values showing enhancements. The effectiveness of the proposed controller and optimization technique is further validated by introducing GRC as nonlinearity in the system. Finally, the robustness of the proposed controller is evaluated through the RSLP. In summary, the study affirms the superior performance of the proposed FOI-PIDF controller, optimized using the WHO algorithm, in LFC for an interconnected two-area nonlinear MSPS.

The main contribution of this research is to propose different controllers based on the FOI technique and optimize their gain parameters through the WHO algorithm. WHO algorithm is applied for the optimization of controller gain parameters of an interconnected two-area MSPS including RES for the first time. The superior performance of this algorithm over commonly used PSO is demonstrated through various case studies. This study can be extended to multi-area multi source power systems including RESs and electric vehicles, and can also be applied to PS in deregulated environment in future research.

Acknowledgment

The authors gave their sincere gratitude to the Ministry of Human Resource Development, Government of India, for providing financial support for the duration of this research work.

References

1) Y. Arya, "Improvement in automatic generation control of two-area electric power systems via a new fuzzy aided optimal pidn-foi controller," *ISA Trans.*, 80 (*May*) 475–490 (2018). doi:10.1016/j.isatra. 2018.07.028.
2) S. Kumar, P.K. Singhal, V. Kumar, and L.K. Sagar, "Optimization of power flow using ga fuzzy approach," *Evergreen*, 10 (*03*) 1549–1557 (2023). doi.org/10.5109/7151702
3) D. Kler, V. Kumar, and K.P.S. Rana, "Optimal integral minus proportional derivative controller design by evolutionary algorithm for thermal-renewable energy-hybrid power systems," *IET Renew. Power Gener.*, 13 (*11*) 2000–2012 (2019). doi:10.1049/iet-rpg.2018.5745.
4) Y. Arya, N. Kumar, P. Dahiya, G. Sharma, E. Çelik, S. Dhundhara, and M. Sharma, "Cascade-iλdμn controller design for agc of thermal and hydro-thermal power systems integrated with renewable energy sources," *IET Renew. Power Gener.*, 15 (*3*) 504–520 (2021). doi:10.1049/rpg2.12061.
5) E. Çelik, and N. Öztürk, "Novel fuzzy 1pd-ti controller for agc of interconnected electric power systems with renewable power generation and energy storage devices," *Eng. Sci. Technol. an Int. J.*, 35 101166 (2022). doi:10.1016/j.jestch.2022.101166.
6) M.M. Rahman, S. Saha, M.Z.H. Majumder, T.T. Suki, M.H. Rahman, F. Akter, M.A.S. Haque, and M.K. Hossain, "Energy conservation of smart grid system using voltage reduction technique and its challenges," *Evergreen*, 9 (*4*) 924–938 (2022). doi:10.5109/6622879.
7) L.K. Sagar, and D.B. Das, "Fuzzy expert system for determining state of solar photo voltaic power plant based on real-time data," *Evergreen*, 9 (*3*) 870–880 (2022). doi.org/10.5109/4843118
8) Shahnawaj, and S. Chanana, "Optimization of lfc controller of two area system integrated with wind energy using hsa," *IEEE Int. Conf. Information, Commun. Instrum. Control. ICICIC 2017*, 1–6 (2018). doi:10.1109/ICOMICON.2017.8279161.
9) S. Shahnawaj, S. Chanana, and R.S. Bhatia, "Improved frequency regulation in microgrids using metaheuristic algorithms," 17 (*2*) 79–90 (2023). doi:10.30486/mjee.2023.1970217.0.
10) P. Dahiya, and A.K. Saha, "Frequency regulation of interconnected power system using black widow optimization," *IEEE Access*, 10 25219–25236 (2022). doi:10.1109/ACCESS.2022.3155201.
11) J.L.K. Grace, A. Maneengam, P.K.V. Kumar, and J. Alanya-Beltran, "Design and implementation of machine learning modelling through adaptive hybrid swarm optimization techniques for machine management," *Evergreen*, 10 (*2*) 1120–1126 (2023). doi:10.5109/6793672.
12) S.U. Umar, and T.A. Rashid, "Critical analysis: bat algorithm-based investigation and application on several domains," *World J. Eng.*, 18 (*4*) 606–620 (2020). doi:10.1108/WJE-10-2020-0495.
13) A.H. Yakout, H. Kotb, H.M. Hasanien, and K.M. Aboras, "Optimal fuzzy pidf load frequency controller for hybrid microgrid system using marine predator algorithm," *IEEE Access*, 9 54220–54232 (2021). doi:10.1109/ACCESS.2021.3070076.
14) S. Oladipo, Y. Sun, and Z. Wang, "Application of a new fusion of flower pollinated with pathfinder algorithm for agc of multi-source interconnected power system," *IEEE Access*, 9 94149–94168 (2021). doi:10.1109/ACCESS.2021.3093084.
15) M. Ali, H. Kotb, M. Kareem AboRas, and H. Nabil Abbasy, "Frequency regulation of hybrid multi-area power system using wild horse optimizer based new combined fuzzy fractional-order pi and tid controllers," *Alexandria Eng. J.*, 61 (*12*) 12187–12210 (2022). doi:10.1016/j.aej.2022.06.008.
16) V. Singh, V.S. Yadav, M. Kumar, and N. Kumar, "Optimization and validation of solar pump performance by matlab simulink and rsm," *Evergreen*, 9 (*4*) 1110–1125 (2022). doi:10.5109/ 6625723.
17) S. Sawant, R.M.R. Ahsan Shah, M. Rahman, A.R. Abd Aziz, S. Smith, and A. Jumahat, "System modelling of an electric two-wheeled vehicle for energy management optimization study," *Evergreen*, 8 (*3*) 642–650 (2021). doi:10.5109/4491656.
18) A. Fathy, and A.G. Alharbi, "Recent approach based movable damped wave algorithm for designing fractional-order pid load frequency control installed in multi-interconnected plants with renewable energy," *IEEE Access*, 9 71072–71089 (2021). doi:10.1109/ACCESS.2021.3078825.
19) E.M. Ahmed, E.A. Mohamed, A. Elmelegi, M. Aly, and O. Elbaksawi, "Optimum modified fractional order controller for future electric vehicles and renewable energy-based interconnected power systems," *IEEE Access*, 9 29993–30010 (2021). doi:10.1109/ACCESS.2021.3058521.
20) E. Sahin, "Design of an optimized fractional high order differential feedback controller for load frequency control of a multi-area multi-source power system with nonlinearity," *IEEE Access*, 8 12327–12342 (2020). doi:10.1109/ACCESS.2020. 2966261.
21) K. Singh, M. Amir, F. Ahmad, and M.A. Khan, "An integral tilt derivative control strategy for frequency control in multimicrogrid system," *IEEE Syst. J.*, 15 (*1*) 1477–1488 (2021). doi:10.1109/JSYST.2020. 2991634.
22) A. Daraz, S.A. Malik, H. Mokhlis, I.U. Haq, F. Zafar, and N.N. Mansor, "Improved-fitness dependent optimizer based foi-pd controller for automatic generation control of multi-source interconnected power system in deregulated environment," *IEEE Access*, 8 197757–197775 (2020). doi:10.1109/ ACCESS.2020.3033983.
23) A.X.R. Irudayaraj, N.I.A. Wahab, M.G.

Umamaheswari, M.A.M. Radzi, N. Bin Sulaiman, V. Veerasamy, S.C. Prasanna, and R. Ramachandran, "A matignon's theorem based stability analysis of hybrid power system for automatic load frequency control using atom search optimized fopid controller," *IEEE Access*, 8 168751–168772 (2020). doi:10.1109/ACCESS.2020.3021212.

24) N. Kumar, B. Tyagi, and V. Kumar, "Application of fractional order pid controller for agc under deregulated environment," *Int. J. Autom. Comput.*, 15 (*1*) 84–93 (2018). doi:10.1007/s11633-016-1036-9.
25) E. Çelik, "Design of new fractional order pi–fractional order pd cascade controller through dragonfly search algorithm for advanced load frequency control of power systems," *Soft Comput.*, 25 (*2*) 1193–1217 (2021). doi:10.1007/s00500-020-05215-w.
26) M. Ali, H. Kotb, K.M. Aboras, and N.H. Abbasy, "Design of cascaded pi-fractional order pid controller for improving the frequency response of hybrid microgrid system using gorilla troops optimizer," *IEEE Access*, 9 150715–150732 (2021). doi:10.1109/ACCESS.2021.3125317.
27) E.M. Ahmed, A. Elmelegi, A. Shawky, M. Aly, W. Alhosaini, and E.A. Mohamed, "Frequency regulation of electric vehicle-penetrated power system using mpa-tuned new combined fractional order controllers," *IEEE Access*, 9 107548–107565 (2021). doi:10.1109/ACCESS.2021.3100800.
28) Y. Arya, "A novel cffopi-fopid controller for agc performance enhancement of single and multi-area electric power systems," *ISA Trans.*, 100 126–135 (2020). doi:10.1016/j.isatra.2019.11.025.
29) I. Naruei, and F. Keynia, "Wild horse optimizer: a new meta-heuristic algorithm for solving engineering optimization problems," *Eng. Comput.*, 38 3025–3056 (2022). doi:10.1007/s00366-021-01438-z.
30) M. Metwally Mahmoud, "Improved current control loops in wind side converter with the support of wild horse optimizer for enhancing the dynamic performance of pmsg-based wind generation system," *Int. J. Model. Simul.*, 00 (*00*) 1–15 (2022). doi:10.1080/02286203.2022.2139128.
31) M. Gheisarnejad, "An effective hybrid harmony search and cuckoo optimization algorithm based fuzzy pid controller for load frequency control," *Appl. Soft Comput. J.*, 65 121–138 (2018). doi:10.1016/j.asoc.2018.01.007.
32) P.C. Sahu, R.C. Prusty, and S. Panda, "Approaching hybridized gwo-sca based type-ii fuzzy controller in agc of diverse energy source multi area power system," *J. King Saud Univ. - Eng. Sci.*, 32 (*3*) 186–197 (2020). doi:10.1016/j.jksues.2019.01.004.
33) A. Daraz, S. Abdullah Malik, I.U. Haq, K.B. Khan, G.F. Laghari, and F. Zafar, "Modified PID controller for automatic generation control of multi-source interconnected power system using fitness dependent optimizer algorithm," 2020. doi:10.1371/journal.pone.0242428.
34) R.K. Sahu, S. Panda, and U.K. Rout, "DE optimized parallel 2-dof pid controller for load frequency control of power system with governor dead-band nonlinearity," *Int. J. Electr. Power Energy Syst.*, 49 (*1*) 19–33 (2013). doi:10.1016/j.ijepes.2012.12.009.
35) Y. Arya, P. Dahiya, E. Çelik, G. Sharma, H. Gözde, and I. Nasiruddin, "AGC performance amelioration in multi-area interconnected thermal and thermal-hydro-gas power systems using a novel controller," *Eng. Sci. Technol. an Int. J.*, 24 (*2*) 384–396 (2021). doi:10.1016/j.jestch.2020.08.015.
36) R.K. Sahu, S. Panda, and S. Padhan, "Optimal gravitational search algorithm for automatic generation control of interconnected power systems," *Ain Shams Eng. J.*, 5 (*3*) 721–733 (2014). doi:10.1016/j.asej.2014.02.004.
37) R.K. Sahu, S. Panda, and G.T. Chandra Sekhar, "A novel hybrid pso-ps optimized fuzzy pi controller for agc in multi area interconnected power systems," *Int. J. Electr. Power Energy Syst.*, 64 880–893 (2015). doi:10.1016/j.ijepes.2014.08.021.
38) T. Veerendar, and D. Kumar, "Teaching-learning optimizer-based fo-pid for load frequency control of interlinked power systems," *Int. J. Model. Simul.*, 00 (*00*) 1–23 (2022). doi:10.1080/02286203.2022.2112009.
39) A.A. Ewees, F.H. Ismail, and R.M. Ghoniem, "Wild horse optimizer-based spiral updating for feature selection," *IEEE Access*, 10 (*October*) 106258–106274 (2022). doi:10.1109/ACCESS.2022.3211263.
40) H.A. Ramadan, B. Khan, and A.A.Z. Diab, "Accurate parameters estimation of three diode model of photovoltaic modules using hunter-prey and wild horse optimizers," *IEEE Access*, 10 (*July*) 87435–87453 (2022). doi:10.1109/ACCESS.2022. 3199001.
41) J. Han, L.M. Bieber, J. Paull, L. Wang, W. Li, and J.N. Paquin, "Real-time simulation of hybrid three-level and modular multilevel converter based on complete equivalent model for high voltage direct current transmission system," *IEEE Open Access J. Power Energy*, 9 (*December 2021*) 42–54 (2022). doi:10.1109/OAJPE.2021.3138345.
42) S. Kumari, and G. Shankar, "Novel application of integral-tilt-derivative controller for performance evaluation of load frequency control of interconnected power system," *IET Gener. Transm. Distrib.*, 12 (*14*) 3550–3560 (2018). doi:10.1049/iet-gtd.2018.0345.

Appendix A

Nominal parameters of the interconnected two-area MSPS [32]:

Rated power, P_{ri} = 2000 MW
Nominal load, P_{L0} = 1500 MW
Power system frequency, f = 60 hz
Frequency bias parameters, $B_{M1} = B_{M2}$ = 0.4312
Regulation parameters, R_i = 2.4 Hz/(pu)MW
Reheat turbine time constant, T_r = 10.2 sec
Reheat turbine gain, K_r = 0.3
Turbine time constant of TES, T_t = 0.3 sec
Governor time constant of TES, T_{gt} = 0.06 sec
Pitch actuator gain of WES, K_P = 1.25
Pitch actuator time constant of WES, T_P = 0.041 sec
Power system time constant, $T_{PS1} = T_{PS2}$ = 11.50 sec
Power System gain, $K_{PS1} = K_{PS2}$ = 68.5426 Hz/(pu)MW
Synchronizing coefficient, T_{12} = 0.0433
Area capacity ratio, a12 = -1
Nominal starting time of water in penstock, T_w = 1.1 sec
Governor time constant of HES, T_{gh} = 0.20 sec
Reset time of HES, T_{rs} = 4.9 sec
Transient droop time constant of hydro turbine, T_{rh} = 28.749 sec
Gas turbine valve positioner, C_g = 1
Gas turbine constant of valve positioner, b_g = 0.049 sec
Combustion reaction time delay of GES , T_{cr} = 0.010 sec
Fuel time constant of GES, T_f = 0.239 sec
Compressor discharge volume time constant of GES, T_{cd} = 0.20 sec
Lead time constant of GES, X_g = 0.60 sec
Lag time constant of GES, Y_g = 1.10 sec

Appendix B

Abbreviation

PS	Power System
MSPS	Multi Source Power System
RESs	Renewable Energy Sources
LFC	Load Frequency Control
ACE	Area Control Error
WES	Wind Energy Systems
HES	Hydro Energy System
TES	Thermal Energy System
GES	Gas Energy System
IAE	Integral of Absolute Error
ITAE	Integral of Time Multiplication of Absolute Error
ISE	Integral of Squared Error
ITSE	Integral of Time Multiplication of Squared Error
PI	Proportional Integral
PID	Proportional Integral Derivative
PIDF	Proportional Integral Derivative with Filter
FCT	Fractional Calculus Theory
FOI	Fractional Order Integral
FOPI	Fractional Order Proportional Integral
FOPD	Fractional Order Proportional Derivative
FOPID	Fractional Order Proportional Integral Derivative
TID	Tilt Integral Derivative
WHO	Wild Horse Optimization
PSO	Particle Swarm Optimization
WOA	Whale Optimization Algorithm
FPA	Flower Pollination Algorithm
ICA	Imperialist Competitive Algorithm
OP	Optimization Problem
FPGA	Field Programmable Gate Arrays
HIL	Hardware in Loop
GRC	Generation Rate Constraint
SLP	Step Load Perturbation
RSLP	Random Step Load Pattern
DRC	Dynamic Response Characteristics
DSO	Digital Storage Oscilloscope